Applied Materials Today 26 (2022) 101337

Contents lists available at ScienceDirect

Applied Materials Today

journal homepage: www.elsevier.com/locate/apmt

Collective behavior of magnetic microrobots through immuno-sandwich assay: On-the-fly COVID-19 sensing

Carmen C. Mayorga-Martinez[a], Jan Vyskočil[a], Filip Novotný[a], Petr Bednar[b,c], Daniel Ruzek[b,d], Osamah Alduhaish[e], Martin Pumera[a,e,f,g,*]

[a] Center for Advanced Functional Nanorobots, Department of Inorganic Chemistry, Faculty of Chemical Technology, University of Chemistry and Technology Prague, Technická 5, Prague 166 28, Czech Republic
[b] Veterinary Research Institute, Hudcova 70, Brno CZ-62100, Czech Republic
[c] Faculty of Science, University of South Bohemia, Branisovska 31, Ceske Budejovice CZ-37005, Czech Republic
[d] Institute of Parasitology, Biology Centre of the Czech Academy of Sciences, Branisovska 31, Ceske Budejovice CZ-37005, Czech Republic
[e] Chemistry Department, College of Science, King Saud University, P. O. Box 2455, Riyadh 11451, Saudi Arabia
[f] Department of Medical Research, China Medical University Hospital, China Medical University, No. 91 Hsueh-Shih Road, Taichung 40402, Taiwan
[g] Department of Food Technology, Center for Nanorobotics and Machine Intelligence, Mendel University in Brno, Zemedelska 1, Brno 61300, Czech Republic

ARTICLE INFO

Article history:
Received 1 September 2021
Revised 4 December 2021
Accepted 19 December 2021

Keywords:
Microrobots
Biosensor
Covid19

ABSTRACT

Mobile self-propelled micro/nanorobots are mobile binding surface that improved the sensitivity of many biosensing system by "on-the-fly" identification and isolation of different biotargets. Proteins are powerful tools to predict infectious disease progression such as COVID-19. The main methodology used to COVID-19 detection is based on ELISA test by antibodies detection assays targeting SARS-CoV-2 virus spike protein and nucleocapside protein that represent an indirect SARS-CoV-2 detection with low sentitivy and specificity. Moreover ELISA test are limited to used external shaker to obtain homogenously immobilization of antibodies and protein on sensing platform. Here, we present magnetic microrobots that collective self-assembly through immuno-sandwich assay and they can be used as mobile platform to detect on-the-fly SARS-CoV-2 virus particle by its spike protein. The collective self-assembly of magnetic microrobots through immuno-sandwich assay enhanced its analytical performance in terms of sensitivity decreasing the detection limit of SARS-CoV-2 virus by one order of magnitude with respect to the devices previously reported. This proof-of-concept of microrobotics offer new ways to the detection of viruses and proteins of medical interest in general.

1. Introduction

Recently, the field of biosensing research has turned its attention to micro/nanorobots that can act as mobile platforms to improve their analytical performance [1–6]. Depending on the material that comprises a micro/nanorobot, bioreceptors such as enzymes, antibodies, aptamers, DNA, and RNA can be immobilized on its surface [2,3,7–9]. The chemistry on-the-fly that micro/nanorobots can be performed, can facilitate the isolation of specific targets even in complex biosamples, avoiding several washing and mixing procedures that require external shakers and centrifuges. Micro/nanorobots are machines that can be propelled by an external stimulus (e.g., light and magnetic/ultrasound fields) [10–18] or by chemical fuels such as H_2O_2, urea, *etc.*, [19–24] thereby providing enhanced diffusion and mixing.

Protein detection based on ELISA immunoassay represent a powerful tool to evaluate different diseases that affect cardiovascular and digestive systems. Moreover, proteins are very well used to identify and evaluate different cancers. Finally, proteins are predictors of infectious disease progression that nowadays play an important role in the world pandemic of acute viral disease, COVID-19 caused by the SARS-CoV-2 virus. However, conventional ELISA immunoassays used to detect SARS-CoV-2 virus are based on immune response test targeting spike (SP) and nucleocapsid (NP) protein. These tests are an indirect detection with low selectivity and sensitivity since the levels of anti-SP and anti-NP antibodies are very low in the early phases of the COVID-19 illness process [25,26].

In this work, we presented a system based on the direct detection of SARS-CoV-2 virus particle by it spike protein that protrudes from the viral envelope and magnetic microrobots (MagRobots) as sensing devices [27]. These MagRobots act as mobile binding sur-

* Corresponding author.
E-mail addresses: oalduhaish@ksu.edu.sa (O. Alduhaish), pumera.research@gmail.com (M. Pumera).

https://doi.org/10.1016/j.apmt.2021.101337
2352-9407/

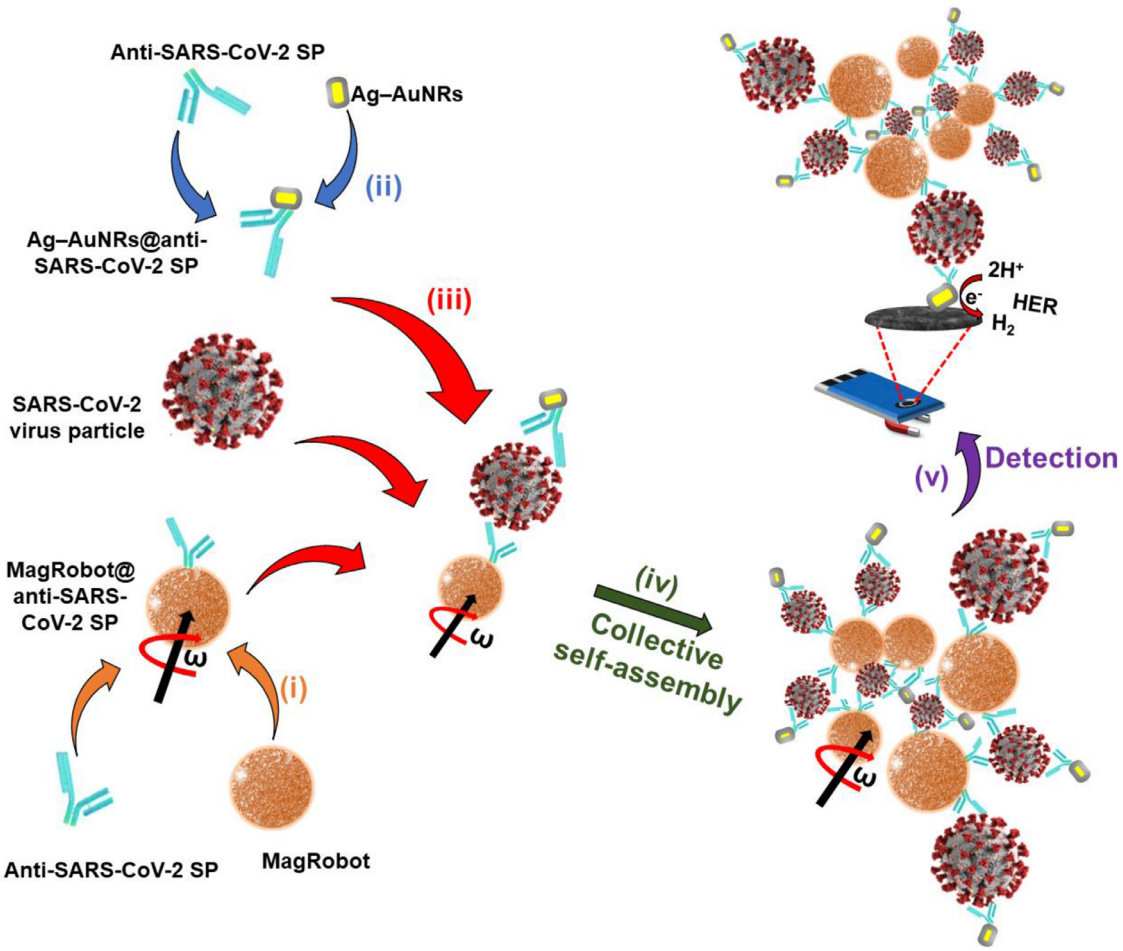

Scheme 1. Schematic representation (not in scale) of (i) MagRobots modified with antibody against SARS-CoV-2 SP that is (iii) driven using transversal rotating magnetic field in presence of SARS-CoV-2 virus particle and (ii) secondary antibody against SARS-CoV-2 SP labelled with Ag–AuNRs (Ag–AuNRs@anti-SARS-CoV-2 SP). (iv) MagRobots shows collective self-assembly through the immuno-sandwich assay of SARS-CoV-2 virus particle. (v)The detection was performed through hydrogen evolution reaction (HER) of Ag–AuNRs.

face where immuno-sandwich assay selective to SARS-CoV-2 virus particle was immobilized. For this purpose, MagRobots were modified with antibody against SARS-CoV-2 spike protein (SP), see (i) Scheme 1. That will be termed in this work as MagRobot@anti-SARS-CoV-2 SP. MagRobot@anti-SARS-CoV-2 SP were used as a mobile platform for the capture of SARS-CoV-2 virus particle and labelled secondary antibody see (iii) Scheme 1. Interestingly, when the immuno-sandwich assay was formed by applied transversal rotating magnetic field, MagRobots were self-assembled and form 3D-staggered chains (see (iv) Scheme 1), while in absence of immuno-sandwich assay, individual or linear chains of MagRobots were observed. This collective self-assembly behavior improves the performance of MagRobots since they walk across a larger area in less time as well as they moved with greater force. In consequence, this collective self-assembly behavior may be responsible for the improvement of its sensitivity by decreasing the detection limit of SARS-CoV-2 virus by an order of magnitude with respect to the device previously reported by Seo et al. [28].

The secondary antibody consists of the antibody against SARS-CoV-2 SP immobilized on the silver-shell/gold-core nanorods(Ag–AuNRs) surface that will be termed as Ag–AuNRs@anti-SARS-CoV-2 SP see (ii) Scheme 1. The detection was performed using a well known detection system that is based on hydrogen evolution reaction (HER) of Ag–AuNRs immobilized on the secondary anti-SARS-CoV-2 SP, (see (v) Scheme 1).

2. Materials and methods

2.1. Reagents and apparatus

To prepare the magnetic immuno-sandwich assay Dynabeads, M-280 tosyl-activated magnetic beads were purchased from Invitrogen, (Czech Republic). Phosphate buffer saline in tablet, boric acid (99.5%), BSA (96%), Tween 20, and human hemoglobin were obtained from (Sigma-Aldrich, Czech Republic) as well as sodium dodecyl sulfate and sodium cholate surfactants. Recombinant SARS-CoV-2/2019-nCoV Spike/RBD protein, SARS-CoV-2/2019-nCoV Spike/RBD antibody and Rabbit PAb were purchased from Sino Biological Europe GmbH.

Electrochemical measurements were performed using SPE electrodes (eDAQ Instruments, Europe) with a three-electrode configuration. An Autolab PGSTAT 204/FRA 32 M (Eco Chemie, Utrecht, The Netherlands) controlled by NOVA version 1.10 software (Eco Chemie) was used to evaluate HER catalysis. Video sequences were recorded using an Olympus CKX53 inverted microscope with a 50X objective lens and Basler acA-1920–155 µm monochrome CMOS camera. Video processing was done using Nikon NIS-Elements software. STEM and SEM micrographs and elemental mapping were done using a field-emission scanning electron microscope (TESCAN MAIA 3) coupled with an energy-dispersive spectrometer (EDS) (Oxford Instruments, UK). Transmission electron microscope JEOL

JEM-1010 at an accelerating voltage of 80 kV was used to obtain TEM images.

MagRobots propulsion under a transversal rotating magnetic field. MagRobots propulsion was evaluated in PBS solution with different surfactants (SDS, Tween 20, and sodium cholate) and BSA. A transversal rotating magnetic field was generated by a home-made magnetic field controlled and using a 3D-printed 6 coils system attached to a microscope table. The magnetic intensity used in all the experiments was 5 mT [29].

2.2. Ag–AuNR synthesis

Silver–gold/core–shell nanorods were synthesized by a two-stage method reported previously [30,31]. A seeded-growth method was used to obtain the core gold nanorods using a solution of silver nitrate and cetyltrimethylammonium bromide (CTAB). To remove excess reagents, the obtained solution was centrifuged, resulting in an Au nanorod pellet that was re-suspended in cetyltrimethylammonium chloride (CTAC) solution (10×10^{-3} M). Afterwards, the silver shell was obtained by adding silver nitrate, sodium hydroxide, and ascorbic acid to the Au nanorod solution and increasing the temperature to 60 °C for 2 h to cause overgrowth of the silver shell. Finally, the solution was cooled to ambient temperature and purified by centrifugation and re-dispersion into CTAC solution (10×10^{-3} M).

2.3. Magneto immuno-sandwich assay preparation

A solution of commercial MagRobots (3 mg mL^{-1}) was washed twice using borate buffer of pH 9.2, added to a solution of anti-SARS-CoV-2 spike protein diluted 5 000 times or 1 000 times from the original solution for detect SARS-CoV-2 spike protein and SARS-CoV-2, respectively. Then incubated overnight at 37 °C with continued agitation at 400 rpm. Next, the obtained solution was washed with PBS pH 7.4 containing Tween 20 at 0.5%. Afterward, the blocking of free spaces of MagRobots were performed using 5% BSA solution in PBS and incubated from 1 h at 25 °C (400 rpm). The obtained solution (conjugated-1) was washed with PBS solution containing 1% BSA. On the other hand, Ag–AuNRs@anti-SARS-CoV-2 spike protein (conjugate-2) was prepared. For that aim, 0.275 nM Ag–AuNRs was mixed with anti-SARS-CoV-2 spike protein antibody solution (5 000 or 1 000 times diluted from the original solution for detect SARS-CoV-2 spike protein and SARS-CoV-2, respectively) and incubated for 60 min, 650 rpm at 25 °C in PBS solution. Afterward, the blocking step was performed by adding 20 µL of 5% BSA solution prepared in PBS to obtain a final volume of 100 µL. This solution was incubated for 20 min, 650 rpm at 25 °C followed by centrifugation at 14,000 rpm for 60 s at 4 °C and re-suspended in PBS. Finally, conjugate-1 and conjugate-2 were placed in a solution of SARS-CoV-2 spike protein or SARS-CoV-2 solutions at different concentration and a transversal rotating magnetic field applied for 30 min. This step was performed in PBS solution containing 0.1% Tween 20. Finally, the obtained solution was washed with PBS and Milli-Q water.

2.4. SARS-CoV-2 and FIPV viral samples preparation

Two representatives of the *Coronaviridae* family, i.e., SARS-CoV-2 (strain SARS-CoV-2/human/Czech Republic/951/2020 isolated from a clinical sample at the National Institute of Health, Prague, Czech Republic, and kindly provided by Dr. Jan Weber, Institute of Organic Chemistry and Biochemistry, Prague, Czech Republic) and feline infectious peritonitis virus (FIPV, ATCC VR990) were used in this study. SARS-CoV-2 was grown in Vero E6 cells (ATCC CRL-1586), cultured in Dulbecco′s modified Eagle′s medium (DMEM) supplemented with 10% newborn calf serum, 100 U/mL penicillin, 100 µg/mL streptomycin, and 1% glutamine (Sigma-Aldrich, Prague, Czech Republic) at 37 °C and 5% CO_2. FIPV was grown in Felis catus kidney cortex cells (CRFK, ATCC CCL-94), cultured in DMEM supplemented with 10% newborn calf serum, 100 U/mL penicillin, 100 µg/mL streptomycin, and 1% glutamine (Sigma-Aldrich, Prague, Czech Republic) at 37 °C and 5% CO_2. The virus titers were determined using plaque assay as described previously [32]. The virus titer was expressed as plaque-forming units (PFU)/ml. Before the use in the experiment, the virus was heat-inactivated by 60 °C for 45 min. The inactivation was confirmed by plaque assay.

2.5. Electrochemical measurement

LSV measurements were performed to evaluate the HER catalysis of Ag-AuNR tags present in the magnetic immuno-sandwich assay using a scan rate of 2 mV s^{-1} in a potential window from 0.2 to 1.2 V vs. RHE. To evaluate the HER result for free Ag–AuNRs, 3 µL of 1.1 nM Ag–AuNRs solution was drop casted onto the working electrode of SP electrode. For SARS-CoV-2 spike protein and SARS-CoV-2 detection, 15 µL of magnetic immuno-sandwich complex was placed and concentrated on the working electrode of SP electrode using an external magnet placed behind it. Afterward, 15 µL of H_2SO_4 was added to obtain a final acid concentration of 0.5 mM; after 1 min, a current was applied at −0.97 V vs. RHE for 50 s.

3. Results and discussion

Paramagnetic particles are an excellent candidate for use as MagRobots due to their unique magnetic properties (see Fig. S1 and Table S1 in the supporting information) and they can be functionalized with diverse functional groups. However, in the micromotors research field, paramagnetic particles are not fully used; typically, they are used for magnetic guidance [33] or to evaluate their collective behavior under a magnetic field [34]. Herein, paramagnetic particles are magnetically driven in order to capture and pre concentrated proteins and virus particles on-the-fly.

First, MagRobots motion under a transversal rotating magnetic field was evaluated. For this aim, Mag Robots motion in different solution were performed, since the immunoassay formation [35] and the microrobots motion [36,37] shown ionic strength dependence. In 10 mM phosphate buffer, pH 7.4 solution (PBS), MagRobots did not show any motion (**see Video S1**) and they remained motionless and attached to the glass surface even at high frequencies, this PBS is a common reagents used to prepare the immunoassay. However, when surfactant such as polyethylene glycol sorbitan monolaurate (Tween 20) and sodium dodecyl sulfate (SDS), were included in the PBS solution, non-motile MagRobots started to rotate and form linear chains (see **Video S2**), surfactants concentrations were at concentration of 1%. Tween 20 was shown as is more efficient additive as allowed microrobots to be detached from the glass surface. Tween 20 is nonionic detergent, which increases the viscosity of the solution and prevents the adhesion of MagRobots to the glass surface. However, Tween 20 is a common surfactant used to immunoassay formation.

MagRobots chains were disassembled when the transversal rotating magnetic field was switched off (see **Video S3**), that observation demonstrated that chains assembled and disassembled of pristine MagRobots depended of transversal rotating magnetic field and it is in agreement with the reported literature [37]. **Video S4** shows the linear motion of MagRobots under a transversal rotating magnetic field at frequencies ranging from 0.5 to 10 Hz. As can be seen, MagRobots assembled and formed linear chains and could homogeneously move at 3 and 5 Hz. However, at 7 and 10 Hz the

MagRobots' motion becomes unstable, and some of them shown tumbling motion.

To prevent MagRobots motion in only one direction and they accumulation in one side of the test tube we have implemented a programed automated motion mode. For this aim, a predefined rectangular trajectory of MagRobots under a transversal rotating magnetic field was used (see **Scheme S1 and Video 5**). In this programed automated mode, MagRobots walk in three rows and two columns and return. **Video S5** shows the predefined rectangular trajectory performed at 5 Hz using magnetic field intensity of 5 mT. When programed automated motion mode was used, MagRobots are well dispersed in the solution. However when they run in just one direction they are accumulate in the side of test tube. See **Video S6** recorded using low magnification objective.

Once the experimental conditions for MagRobots propulsion were optimized, the immuno-sandwich assay was optimized using spike protein of SAR-CoV-2 (SAR-CoV-2 SP). Briefly, tosyl-activated MagRobots were conjugated with anti-SARS-CoV-2 SP to obtain MagRobots@anti-SAR-CoV-2 SP, see Scheme 1(i) and materials and methods section. In parallel, the anti-SARS-CoV-2 SP is also immobilized on the surface of Ag–AuNRs to obtain Ag–AuNRs@anti-SARS-CoV-2 SP (Scheme 1 (ii). Afterwards, MagRobots@anti-SAR-CoV-2 SP and Ag–AuNRs@anti-SARS-CoV-2 SP conjugates were placed in the presence of SARS-CoV-2 spike protein to the desired concentration and predefined rectangular trajectories under a transversal rotating magnetic field at 5 Hz and 5mTwas run for 30 min (see Scheme 1 (iii)). Herein, we take advantage of micromixing generated by the magnetic propulsion of MagRobots@anti-SAR-CoV-2 SP to complete the immuno-sandwich assay. **Video S6** shows predefined rectangular trajectories under a transversal rotating magnetic field of MagRobots@anti-SARS-CoV-2 SP/SARS-CoV-2 SP/Ag–AuNRs@anti-SARS-CoV-2 SP. In this video, it can be clearly seen that when is formed the complete magneto immuno-sandwich assay; MagRobots were assembled forming 3D-staggered chains in instead of linear chains (see Scheme 1 (iv) and Video S7). These collective self-assembly MagRobots through immuno-sandwich assay is extraordinarily strong and cannot be disassembled even when the transversal rotating magnetic field is off. These 3D-staggered chains MagRobots were faster that the individual MagRobots, moreover this strong motion avoid the precipitation of MagRobots to the bottom of test tubes and increasing the micromixing effect.

Transmission electron microscopy (TEM) and energy-dispersive X-ray spectroscopy (EDS) analysis were carried out to evaluate the self-assembly of MagRobots through the immuno-sandwich assay. For this aim, TEM of MagRobots@anti-SARS-CoV-2 SP/SARS-CoV-2 SP/Ag–AuNRs@anti-SARS-CoV-2 SP and pristine MagRobots were compared, in both cases transversal rotating field using programed automated mode was applied for 30 min at 5 Hz and 5 mT. **Fig. 1A** shows TEM images of MagRobots@anti-SARS-CoV-2 SP/SARS-CoV-2 SP/Ag–AuNRs@anti-SARS-CoV-2 SP that clearly are self-assembled. Whereas, in absence of immuno-sandwich assay, pristine MagRobots did not assembled and isolated microparticles were observed (**Fig. 1B**). In addition, the presence of Ag-AuNRs were observed by EDS elementary mapping analysis (**Fig. 1C**) and its EDS spectrum (**Fig. S2A)** of MagRobots@anti-SARS-CoV-2 SP/SARS-CoV-2 SP/Ag–AuNRs@anti-SARS-CoV-2 SP conjugate. Clearly, signal of Au and Ag were only observed on the surface of MagRobots@anti-SARS-CoV-2 SP/SARS-CoV-2 SP/Ag–AuNRs@anti-SARS-CoV-2 SP (Figs. 1C and S2A). Moreover, the total absence of au and Ag was demonstrated on EDS spectrum of pristine MagRobots (Fig. S2B).

To perform SARS-CoV-2 SP and SARS-CoV-2 virus particle detection, Ag–AuNRs were used as electro-catalytic label. Ag–AuNRs were prepared via seeded-growth method of gold nanorods in the presence of silver nitrate (see Materials and Methods section) [30,31]. The morphological and chemical characterized of Ag–AuNRs were performed by scanning transmission electron microscopy (STEM) and energy-dispersive X-ray spectroscopy (EDS). The STEM and STEM high-angle dark-field retractable (STEM-HADF) micrographs (**Fig. 2A** and **2B**) show uniform size and shape distribution of Ag–AuNRs, whereas EDS elemental mapping from the SEM image show that Ag–AuNRs have a uniform silver outer layer with a uniform gold core (**Fig. 2C**). In addition, the size distribution obtained from STEM images reveals homogeneous rectangular-shaped Ag–AuNRs with average length and width of 69.4 ± 9.3 nm and 39 ± 4.9 nm, respectively (see **Fig. 2D**). Moreover, Ag–AuNRs show an average Ag outside layer thickness of 12.6 ± 2.9 nm. In addition, the ultraviolet-visible (UV–Vis) spectrum (**Fig. 3A**) of Ag–AuNRs is in good agreement with values reported previously, [31] with a particle concentration of 1.1 nM.

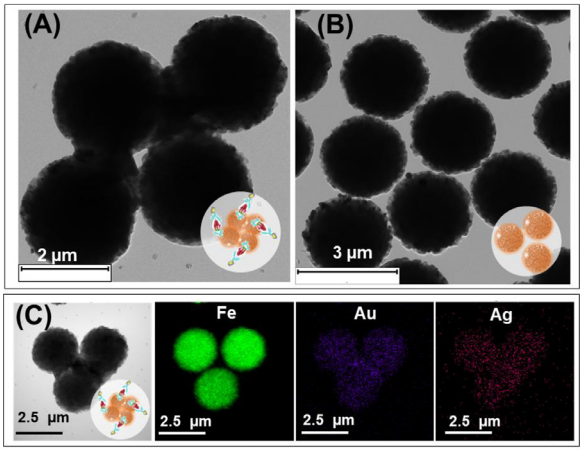

Fig. 1. TEM images of MagRobots@anti-SARS-CoV-2 SP/SARS-CoV-2 SP/Ag–AuNRs@anti-SARS-CoV-2 SP conjugate (A) and pristine MagRobots (B). EDX elementary mapping from TEM images of Ag–AuNRs@anti-SARS-CoV-2SP/SARS-CoV-2SP/ MagRobots @anti-SARS-CoV-2 SP (C).

After the Ag–AuNRs were morphologically characterized, hydrogen evolution reaction (HER) catalysis was performed using linear sweep voltammetry (LSV) of screen-printed electrode modified with Ag–AuNRs. HER is a cathodic half reaction of water splitting and is used in many applications such energy conversion devices, artificial photosynthetic cells and biosensing [3,38–40]. In addition, LSV of an unmodified SP electrode was recorded as a control. The resulting LSV curves were compared in **Fig. 3B**. Ag–AuNRs reveal enhanced HER performance with an onset potential of −0.97 V vs. RHE at −10 mA/cm^2. In addition, Ag–AuNRs with different Ag side thickness were compared see **Fig. S3**. Improved HER performance was observed in Ag–AuNRs with Ag side thickness of 8.7 nm (line red); this NRs were used in the following experiment.

Once the Ag–AuNRs@anti-SARS-CoV-2SP/SARS-CoV-2SP/MagRobots@anti-SARS-CoV-2 SP is formed, sensing was performed through HER catalysis of Ag–AuNRs. For this aim, magneto immuno-sandwich assay was placed and concentrated on the working electrode (WE) of SP electrode by external magnet placed behind the WE. Then, H_2SO_4 0.5 M was added, see details in experimental section. Finally, chronoamperogram was recorded for 50 s by applying −0.97 V vs. RHE, the onset potential of HER of Ag–AuNRs. Two sets of control experiments were performed to evaluate the performance of the magnetic immuno-sandwich assay developed here. The first control experiment was performed in conventional conditions to prepare the magnetic immuno-sandwich assay using external shaking and the second one was performed in static mode; both controls were compared with the mobile mode. The recorded current from HER catalysis of all experiments were compared in **Fig. 4A**. Clearly, the enhanced current

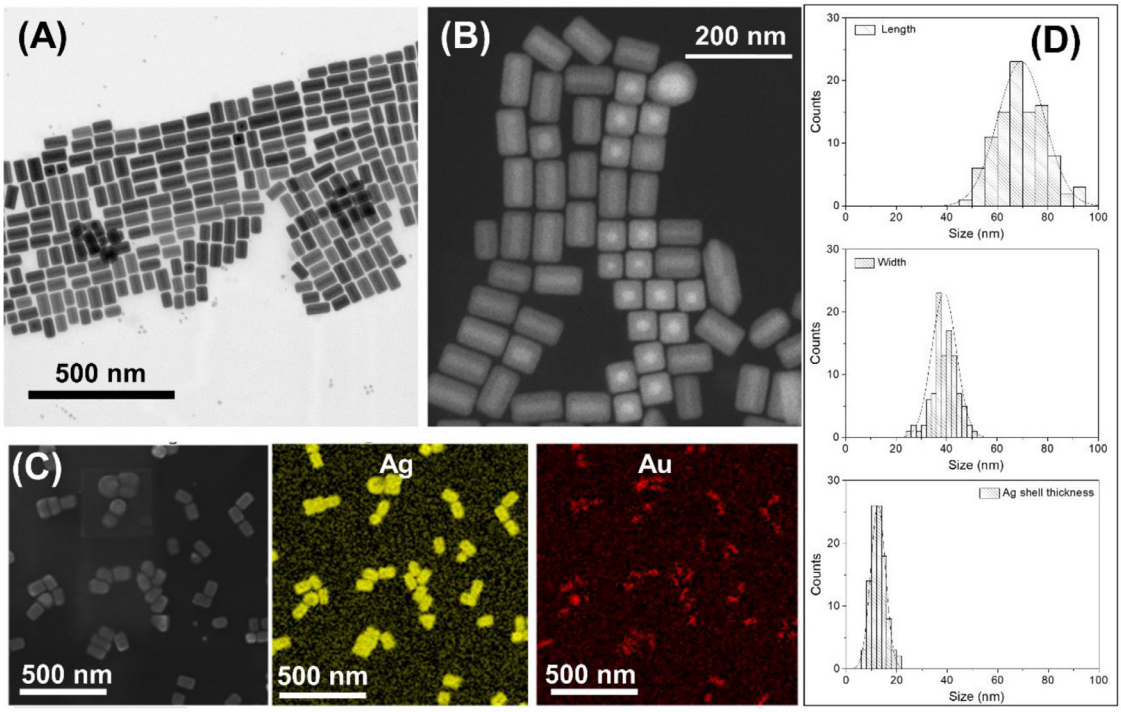

Fig. 2. Morphological characterization of Ag–AuNRs. STEM images (A), STEM-HADF image (B), and EDS elementary mapping from SEM images (C) of Ag–AuNRs. Length, width, and Ag shell thickness distribution of Ag–AuNRs (D).

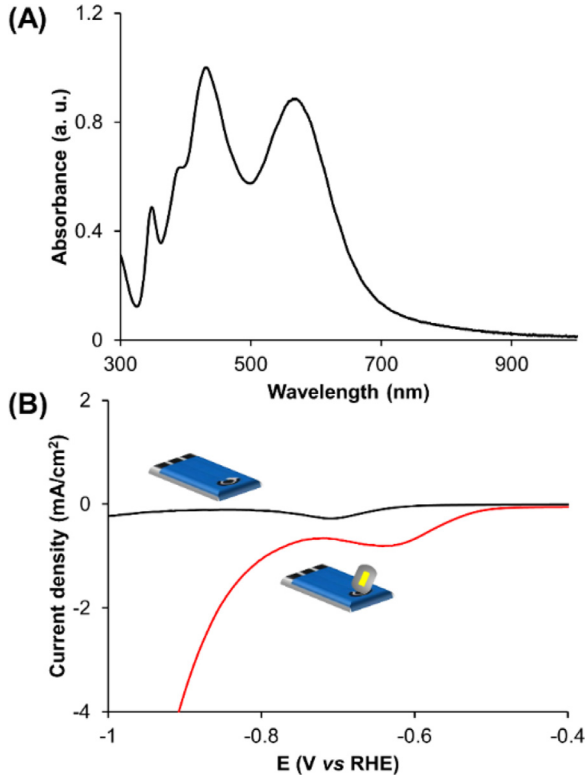

Fig. 3. Optical and catalytic characterization of Ag–AuNRs. UV–Vis spectrum of Ag–AuNRs (A) and LSV curves of Ag–AuNRs (red line) and SP electrode bare (black line) (B).

intensity was observed in MagRobots propelled under transversal rotating magnetic field using programed automated motion mode (see red column, dynamic). In addition, low current intensity were observed when external shaker was used (see blue column), and the lowest current intensity was observed in static mode (yellow column). The incubation time used was 30 min to be comparable with the MagRobot in dynamic mode. In all experiment 500 ng/mL SARS-CoV-2 spike protein was used. According to One-Way ANOVA test statistical analysis with a confidence interval of 95%, the mean values for immune-sandwich assay of SARS-Cov-2 SP prepared in static and dynamic modes as well as using external shakers were statistically different with $p = 0.00004$. The plausible reason, that dynamic mode is more efficient to external shaker is because antibodies can aggregated under shaking producing mechanical stress on them [41]. Moreover, we have observed that MagRobots partially precipitate to the bottom of test tube under shaker mode.

Different mixing times were used to optimize the detection of SAR-CoV-2 virus particle. 30 min was used since at 15 min the sensitivity decreases and at 45 min the sensitivity not change (data not shown). Moreover, different concentration Ag-AuNRs (0.138, 0.275 and 0.413 nM) were evaluated to prepare the immunoassay and not significant differences were observed. However, in the following experiments 0.275 nM Ag-AuNRs was used because this concentration showed a slightly improved result see **Fig. S4 (A)**. In addition, immunoassays prepared using Ag–AuNRs with different Ag side thickness were compared higher signal was observed when Ag–AuNRs with Ag side thickness of 8.7 nm was used; see Fig. S4 (B). In all cases 500 ng/mL SARS-CoV-2 spike protein was used.

In addition, selectivity assay was performed (see **Fig. 4B**). In the presence of 1000 ng/mL hemoglobin (Hb) instead of 500 ng/mL SARS-CoV-2 spike protein. When the immuno-sandwich assay was performed in presence of Hb, the system shows lower current intensity even when concentration of Hb was twice of SARS-CoV-2 spike protein concentration. According to *t*-test statistical analysis with a confidence interval of 95%, the mean values for immune-sandwich assay of SARS-Cov-2 SP and Hb were very statistically different with $p = 0.0031$. Finally, the calibration curve of current recorded from HER catalysis as a function of different concentration of SARS-CoV-2 spike protein is presented in **Fig. 4C**. A range from 0.5 to 500 nM was obtained ($r = 0.99$) with a limit of detec-

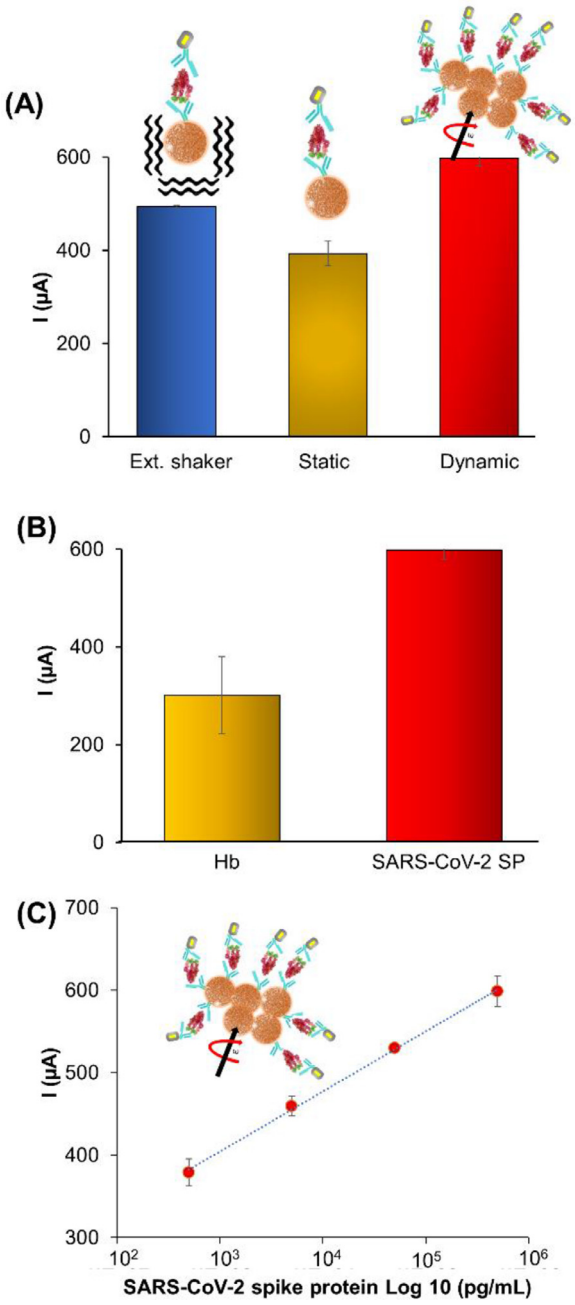

Fig. 4. (A) HER catalysis of self-assembled MagRobots through immuno-sandwich assay prepared under external shaker (blue column), dynamic mode (red column) and static mode (yellow column). (B) Selectivity assay of self-assembled MagRobots through immuno-sandwich assay, hemoglobin (Hb) was used instead of SARS-CoV-2 spike protein (SARS-CoV-2 SP). (C) Calibration curve of SARS-CoV-2 spike protein at different concentration as a function of current intensity obtained from HER catalysis of Ag–AuNRs used as labels in the self-assembled MagRobots through immuno-sandwich assay. Experimental conditions: In (A) 500 pg/mL SARS-CoV-2 SP was used in all experiments. In (B) 500 ng/mL of SARS-CoV-2 SP and 1000 pg/mL of hemoglobin (Hb) were used. In all experiments, 30 min of incubation time were used.

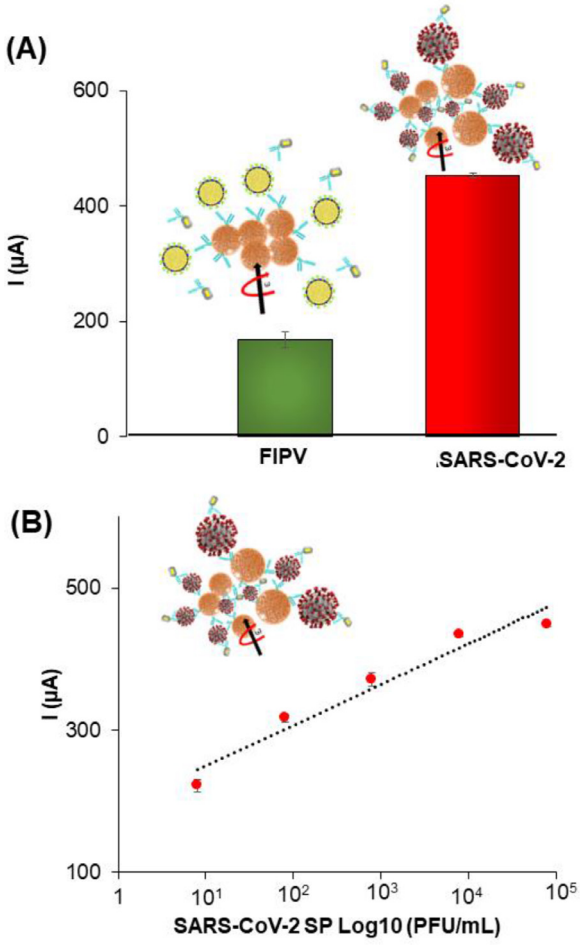

Fig. 5. (A) Selectivity assay of self-assembled MagRobots through immuno-sandwich assay to detect SARS-CoV-2 using feline infectious peritonitis virus particle (FIPV) instead of SARS-CoV-2 virus particle. (B) Calibration curve of SARS-CoV-2 at different concentration as a function of current obtained from HER catalysis of Ag–AuNRs. Experimental conditions: In (A) 8000 PFU/mL of FIPV and SARS-CoV-2 virus particles was used. In all experiments, 30 min of incubation time were used.

tion (LOD) of 1.56 pg/mL and enhanced reproducibility with relative standard deviation (RSD) of 3.21%. RSD is the mean of three repetitions and for four different concentrations. The wide detection range reported here allows to obtain low LOD to detect SARS-CoV-2 spike protein that it is very similar to that reported for detecting IgG (model protein for immunoassay systems) using bubble propelled micromotors [3]. However, the greatest advantage of the system reported in this paper is that these MagRobots do not need any non-biocompatible and toxic fuel that can denature the proteins and antibodies.

Finally, the detection of heat-inactivated authentic SARS-CoV-2 was performed. For this aim, Ag–AuNRs@anti-SARS-CoV-2SP/SARS-CoV-2/MagRobots@anti-SARS-CoV-2 SP conjugate was prepared in similar way as for the spike protein (see materials and methods section). First, we performed the selectivity assay, when SARS-CoV-2 and feline infectious peritonitis virus (FIPV; member of genus *Alphacoronavirus*, family *Coronaviridae*) [42] was used (see Fig. 5A). As can be seen in Fig. 5A, our developed system based on self-assembled MagRobots through immuno-sandwich assay shows enhanced selectivity for SARS-CoV-2 compared to another coronavirus. In these experiments, the same concentration (8000 PFU/mL) of both virus particles was used as well as the same incubation time (30 min). According to *t*-test statistical analysis with a confidence interval of 95%, the mean values for immune-sandwich assay of SARS-Cov-2 and FIPV were extremely statistically different with $p = 0.0001$.

In addition, calibration curve of current recorded from HER catalysis as a function of different concentration of SARS-CoV-2 was performed (Fig. 5B). A linear range was observed from 8 to 8×10^4 PFU/mL, with $r = 0.9733$. This system shows as low detection limit (LOD) as of 1.11 PFU/mL and high reproducibility with

relative standard deviation (RSD) of 1.97%. The LOD reported in this work is one order of magnitude lower that to the one reported by Seo et al. [28] They detected SARS-CoV-2 virus particles using a field-effect transistor that needed more complex system to record the sensing signal that the one that we used in this work.

4. Conclusion

Here we have prepared self-assembled MagRobots through immuno-sandwich assay. MagRobots modified with anti-SARS-CoV-2 spike protein were used to load and pre-concentrate SARS-CoV-2 by its spike protein and anti-SARS-CoV-2 spike protein conjugation with Ag–AuNRs were used as labels. The detection was performed through the HER electrocatalysis of Ag–AuNRs. This conceptually new microrobotic scheme for sensing of virus and proteins can be applied to any similar virus or protein detection.

Declaration of Competing Interest

"There are no conflicts to declare".

CRediT authorship contribution statement

Carmen C. Mayorga-Martinez: Conceptualization, Project administration, Investigation, Visualization, Formal analysis, Validation, Writing – original draft, Writing – review & editing. **Jan Vyskočil:** Methodology, Investigation, Resources, Writing – review & editing. **Filip Novotný:** Visualization, Investigation, Writing – review & editing. **Petr Bednar:** Validation, Investigation, Writing – review & editing. **Daniel Ruzek:** Validation, Writing – review & editing. **Osamah Alduhaish:** Supervision, Funding acquisition, Writing – review & editing. **Martin Pumera:** Supervision, Resources, Writing – review & editing.

Acknowledgements

This work was supported by the Distinguished Scientist Fellowship Program (DSFP) of King Saud University, Riyadh, Saudi Arabia.

Supplementary materials

Supplementary material associated with this article can be found, in the online version, at doi:10.1016/j.apmt.2021.101337.

References

[1] S. Campuzano, B. Esteban-Fernández de Ávila, P. Yáñez-Sedeño, J.M. Pingarrón, J. Wang, Nano/microvehicles for efficient delivery and (bio)sensing at the cellular level, Chem. Sci. 8 (2017) 6750–6763.
[2] B. Esteban-Fernández de Avila, A. Martín, F. Soto, M.A. Lopez-Ramirez, S. Campuzano, G.M. Vásquez-Machado, W. Gao, L. Zhang, J. Wang, Single cell real–time miRNAs sensing based on nanomotors, ACS Nano 9 (2015) 6756–6764.
[3] C.C. Mayorga-Martinez, M. Pumera, Self-propelled tags for protein detection, Adv. Funct. Mater. 30 (2020) 1906449.
[4] M. Pacheco, B. Jurado-Sánchez, A. Escarpa, Sensitive monitoring of enterobacterial contamination of food using self-propelled Janus microsensors, Anal. Chem. 90 (2018) 2912–2917.
[5] M. Pacheco, M.Á. López, B. Jurado-Sánchez, A. Escarpa, Self-propelled micromachines for analytical sensing: a critical review, Anal. Bioanal. Chem. 411 (2019) 6561–6573.
[6] K. Yuan, M.Á. López, B. Jurado-Sánchez, A. Escarpa, Janus micromotors coated with 2D nanomaterials as dynamic interfaces for (bio)-sensing, ACS Appl. Mater. Interfaces 12 (2020) 46588–46597.
[7] B. Jurado-Sánchez, A. Escarpa, Milli, micro and nanomotors: novel analytical tools for real-world applications, Trends Anal. Chem. 84 (2016) 48–59.
[8] E. Karshalev, B. Esteban-Fernandez de Avíla, J. Wang, Micromotors for "chemistry-on-the-fly, J. Am. Chem. Soc. 140 (2018) 3810–3820.
[9] J. Li, M. Pumera, 3D printing of functional microrobots, Chem. Soc. Rev. 50 (2021) 2794–2838, doi:10.1039/D0CS01062F.
[10] X.-Z. Chen, B. Jang, D. Ahmed, C. Hu, De Marco C, M. Hoop, F. Mushtaq, B.J. Nelson, S. Pané, Small-scale machines driven by external power sources, Adv. Mater. 30 (2018) 1705061.
[11] C.C. Mayorga-Martinez, J. Vyskočil, F. Novotný, M. Pumera, Light-driven Ti_3C_2 MXene micromotors: self-propelled autonomous machines for photodegradation of nitroaromatic explosives, J. Mater. Chem. A 9 (2021) 14904–14910.
[12] F. Mushtaq, M. Guerrero, M.S. Sakar, M. Hoop, A. Lindo, J. Sort, X. Chen, B.J. Nelson, E. Pellicer, S. Pané, Magnetically driven Bi_2O_3/BiOCl-based hybrid microrobots for photocatalytic water remediation, J. Mater. Chem. A 3 (2015) 23670–23679.
[13] J. Li, T. Li, T. Xu, M. Kiristi, W. Liu, Z. Wu, J. Wang, Magneto–acoustic hybrid nanomotor, Nano Lett. 15 (2015) 4814–4821.
[14] M. Dong, X. Wang, X.-Z. Chen, F. Mushtaq, S. Deng, C. Zhu, H. Torlakcik, A. Terzopoulou, X.-H. Qin, X. Xiao, J. Puigmartí-Luis, H. Choi, A.P. Pêgo, Q.-D. Shen, B.J. Nelson, S. Pané, 3D-Printed soft magnetoelectric microswimmers for delivery and differentiation of neuron-like cells, Adv. Funct. Mater. 30 (2020) 1910323.
[15] B. Jang, A. Hong, H.E. Kang, C. Alcantara, S. Charreyron, F. Mushtaq, E. Pellicer, R. Büchel, J. Sort, S.S. Lee, B.J. Nelson, S. Pané, Multiwavelength light-responsive Au/B-TiO2 Janus micromotors, ACS Nano 11 (2017) 6146–6154.
[16] G. Chatzipirpiridis, C. de Marco, E. Pellicer, O. Ergeneman, J. Sort, B.J. Nelson, S. Pané, Template-assisted electroforming of fully semi-hard-magnetic helical microactuators, Adv. Eng. Mater. 20 (2018) 1800179.
[17] H. Gu, Q. Boehler, H. Cui, E. Secchi, G. Savorana, C. De Marco, S. Gervasoni, Q. Peyron, T.Y. Huang, S. Pane, A.M. Hirt, D. Ahmed, B.J. Nelson, Magnetic cilia carpets with programmable metachronal waves, Nat. Commun. 11 (2020) 2637.
[18] C.C.J. Alcantara, S. Kim, S. Lee, B. Jang, P. Thakolkaran, J.Y. Kim, H. Choi, B.J. Nelson, S. Pané, 3D Fabrication of fully iron magnetic microrobots, Small 15 (2019) 1805006.
[19] R. Mundaca-Uribe, B. Esteban-Fernández de Ávila, M. Holay, P.L. Venugopalan, B. Nguyen, J. Zhou, A. Abbas, R.H. Fang, L. Zhang, J. Wang, Zinc microrocket pills: fabrication and characterization toward active oral delivery, Adv. Healthc. Mater. 9 (2020) 2000900.
[20] S. Tang, F. Zhang, H. Gong, F. Wei, J. Zhuang, E. Karshalev, B. Esteban-Fernández de Ávila, C. Huang, Z. Zhou, Z. Li, L. Yin, H. Dong, R.H. Fang, X. Zhang, L. Zhang, J. Wang, Enzyme-powered Janus platelet cell robots for active and targeted drug delivery, Sci. Robot. 5 (2020) eaba6137.
[21] B. Esteban-Fernández de Ávila, M.A. Lopez-Ramirez, R. Mundaca-Uribe, X. Wei, D.E. Ramírez-Herrera, E. Karshalev, B. Nguyen, R.H. Fang, L. Zhang, J. Wang, Multicompartment tubular micromotors toward enhanced localized active delivery, Adv. Mater. 32 (2020) 2000091.
[22] F. Soto, E. Karshalev, F. Zhang, B.E. Fernandez de Avila, A. Nourhani, J. Wang, Smart materials for microrobots, Chem. Rev. (2021), doi:10.1021/acs.chemrev.0c00999.
[23] H. Wang, M. Pumera, Fabrication of micro/nanoscale motors, Chem. Rev. 115 (2015) 8704–8735.
[24] W. Gao, S. Sattayasamitsathit, K.M. Manesh, D. Weihs, J. Wang, Magnetically powered flexible metal nanowire motors, J. Am. Chem. Soc. 132 (2010) 14403–14405.
[25] T. Ji, Z. Liu, G.Q. Wang, X. Guo, S.A. khan, C. Lai, H. Chen, S. Huang, S. Xia, B. Chen, H. Jia, Y. Chen, Q. Zhou, Detection of COVID-19: a review of the current literature and future perspectives, Biosens. Bioelectron. 166 (2020) 112455.
[26] K.P.A. Kumar, M. Pumera, 3D-Printing to Mitigate COVID-19 Pandemic, Adv. Funct. Mater. 31 (22) (2021) 2100450, doi:10.1002/adfm.202100450.
[27] H. Zhou, C.C. Mayorga-Martinez, S. Pane, L. Zhang, M. Pumera, Magnetically Driven Micro and Nanorobots, Chem. Rev. 121 (8) (2021) 4999–5041, doi:10.1021/acs.chemrev.0c01234.
[28] G. Seo, G. Lee, M.J. Kim, S.H. Baek, M. Choi, K.B. Ku, C.S. Lee, S. Jun, D. Park, H.G. Kim, S.J. Kim, J.O. Lee, B.T. Kim, E.C. Park, S.I. Kim, Rapid detection of COVID-19 causative virus (SARS-CoV-2) in human nasopharyngeal swab specimens using field-effect transistor-based biosensor, ACS Nano 14 (2020) 5135–5142.
[29] J. Vyskočil, C.C. Mayorga-Martinez, E. Jablonská, F. Novotný, T. Ruml, M. Pumera, Cancer cells microsurgery via asymmetric bent surface Au/Ag/Ni microrobotic scalpels through a transversal rotating magnetic field, ACS Nano 14 (2020) 8247–8256.
[30] H.L. Chia, C.C. Mayorga-Martinez, R. Gusmão, F. Novotny, R.D. Webster, M. Pumera, A highly sensitive enzyme-less glucose sensor based on pnictogens and silver shell–gold core nanorod composites, Chem. Commun. 56 (2020) 7909–7912.
[31] F. Novotný, J. Plutnar, M. Pumera, Plasmonic self-propelled nanomotors for explosives detection via solution-based surface enhanced Raman scattering, Adv. Funct. Mater. 29 (2019) 1903041.
[32] M. Stefanik, P. Strakova, J. Haviernik, A.D. Miller, D. Ruzek, L. Eyer, Antiviral activity of vacuolar ATPase blocker diphyllin against SARS-CoV-2, Microorganisms 9 (2021) 471.
[33] M. Luo, S. Li, J. Wan, C. Yang, B. Chen, J. Guan, Enhanced propulsion of urease-powered micromotors by multilayered assembly of ureases on janus magnetic microparticles, Langmuir (2020), doi:10.1021/acs.langmuir.9b03315.
[34] K. Villa, L. Krejčová, F. Novotný, Z. Heger, Z. Sofer, M. Pumera, Cooperative multifunctional self-propelled paramagnetic microrobots with chemical handles for cell manipulation and drug delivery, Adv. Funct. Mater. 28 (2019) 1804343.
[35] K.L. Cox, V. Devanarayan, A. Kriauciunas, J. Manetta, C. Montrose, Sitta Sittampalam, et al., Immunoassay Methods, in: S. Markossian, A. Grossman, K. Brimacombe, et al. (Eds.), Eli Lilly & Company and the National Center For Advancing Translational Sciences, 2004.

[36] X. Arqué, X. Andrés, R. Mestre, B. Ciraulo, J.O. Arroyo, R. Quidant, T. Patiño, S. Sánchez, Ionic species affect the self-propulsion of urease-powered micromotors, Research 2020 (2020) 2424972.
[37] J. Yu, D. Jin, K.-.F. Chan, Q. Wang, L.Zhang K.Yuan, Active generation and magnetic actuation of microrobotic swarms in bio-fluids, Nat Commun. 10 (2019) 5631.
[38] J.O'M. Bockris, E.C. Potter, The mechanism of the cathodic hydrogen evolution reaction, J. Electrochem. Soc. 99 (1952) 169–186.
[39] P.C.K. Vesborg, B. Seger, I. Chorkendorff, Recent development in hydrogen evolution reaction catalysts and their practical implementation, Phys. Chem. Lett. 6 (2015) 951–957.
[40] C.C. Mayorga-Martinez, B. Khezri, A.Y.S. Eng, Z. Sofer, P. Ulbrich, M. Pumera, Bipolar electrochemical synthesis of WS_2 nanoparticles and their application in magneto-immunosandwich assay, Adv. Funct. Mater. 26 (2016) 4094–4098.
[41] S. Kiese, A. Papppenberger, W. Friess, H.-.C. Mahler, Not stirred: mechanical stress testing of an IgG1 antibody, J. Pharm. Sci. 10 (2008) 4347–4366.
[42] N.C. Pedersen, A review of feline infectious peritonitis virus infection: 1963-2008, J. Feline Med. Surg. 11 (2009) 225.